1-1-2014

Effect of stress state on deformation and fracture of nanocrystalline copper: molecular dynamics simulation

Liang Zhang
University of Wollongong, lz592@uowmail.edu.au

Cheng Lu
University of Wollongong, chenglu@uow.edu.au

A Kiet Tieu
University of Wollongong, ktieu@uow.edu.au

Linqing Pei
University of Wollongong, lp115@uowmail.edu.au

Xing Zhao
University of Wollongong, xz920@uowmail.edu.au

Effect of stress state on deformation and fracture of nanocrystalline copper: molecular dynamics simulation

Abstract

Deformation in a microcomponent is often constrained by surrounding joined material making the component under mixed loading and multiple stress states. In this study, molecular dynamics (MD) simulation are conducted to probe the effect of stress states on the deformation and fracture of nanocrystalline Cu. Tensile strain is applied on a Cu single crystal, bicrystal and polycrystal respectively, under two different tension boundary conditions. Simulations are first conducted on the bicrystal and polycrystal models without lattice imperfection. The results reveal that, compared with the performance of simulation models under free boundary condition, the transverse stress caused by the constrained boundary condition leads to a much higher tensile stress and can severely limit the plastic deformation, which in return promotes cleavage fracture in the model. Simulations are then performed on Cu single crystal and polycrystal with an initial crack. Under constrained boundary condition, the crack tip propagates rapidly in the single crystal in a cleavage manner while the crack becomes blunting and extends along the grain boundaries in the polycrystal. Under free boundary condition, massive dislocation activities dominate the deformation mechanisms and the crack plays a little role in both single crystals and polycrystals.

Disciplines

Engineering | Science and Technology Studies

Publication Details

Zhang, L., Lu, C., Kiet, T., Pei, L. & Zhao, X. (2014). Effect of stress state on deformation and fracture of nanocrystalline copper: molecular dynamics simulation. Chinese Physics B, 23 (9), 098102-1-098102-8.

Effect of Stress State on Deformation and Fracture of Nanocrystalline Copper by Molecular Dynamics Simulation*

Zhang Liang(张亮)†, Lu Cheng(吕程) †, Kiet Tieu, Pei Lin-Qing(裴林清), Zhao Xing(赵星)

School of Mechanical, Materials and Mechatronic Engineering, University of Wollongong, Wollongong, NSW 2522, Australia

*Project supported by Australia Research Council Discovery Projects Grant (DP0773329)

† Corresponding author. E-mail: chenglu@uow.edu.au

Deformation in a microcomponent is often constrained by surrounding joined material and then makes the component under mixed loading and multiple stress state. In this study, molecular dynamics (MD) simulation are conducted to probe the effect of stress state on the deformation and fracture of nanocrystalline Cu. Tensile strain is applied on Cu single crystal, bicrystal and polycrystal respectively under two different tension boundary conditions. Simulations are firstly conducted on the bicrystal and polycrystal model without lattice imperfection. The results reveal that, compared with the performance of simulation models under free boundary condition, the transverse stress caused by the constrained boundary condition leads to a much higher tensile stress and can severely limit the plastic deformation, which in return promote cleavage fracture in the model. Simulations are then performed on Cu single crystal and polycrystal with initial crack. Under constrained boundary condition, the crack-tip propagates rapidly in the single crystal in a cleavage manner while the crack becomes blunting and extends along the grain boundaries in the polycrystal. Under free boundary condition, massive dislocation activities dominate the deformation mechanisms and the crack plays a little role in both single crystal and polycrystal.

Keywords: molecular dynamics, nanocrystalline, stress state, deformation mechanism

PACS: 81.07.Nb, 81.07.Bc, 81.40.Vw, 81.40.Jj

1. Introduction

Many next generation micro-electromechanical systems, nano-electromechanical systems and other micro-devices are being researched and they are widely applied to the production practice, their performance and reliability is contingent on the materials from which they are composed. Therefore, it is crucial to develop a sound understanding of deformation in materials with sub-micrometer dimensions. Compared with conventional coarser grained materials, nanostructure materials have a number of superior mechanical properties of potential significance for structure applications, including the high yield and fracture strength [1, 2], superior wear resistance [3-5], and high fatigue resistance [6-10] etc. The appealing mechanical characteristics of nanostructure material has provoked the great interests of researchers to explore its mechanical properties and underlying deformation mechanisms. Because the atomistic mechanisms are very hard to quantify experimentally, computer simulations based on atomistic models has became a powerful tool for gaining the fundamental knowledge in the past two decades and the results have been productive.

The properties and deformation mechanisms of nanocrystalline materials have been primarily studied with a focus on the impact of grain size [11-19]. The dislocation activities in the interior of grains lessen when the average grain size is less than 100 nm whereas mechanisms mediated by the grain boundary become dominant. However, not only the grain size but also the stress state can dramatically influence the mechanical response of nanocrystalline materials [20]. For example, hydrostatic pressure is determined that can improve the plasticity of metal during plastic forming process. Unfortunately, most of the previous research work conducted by atomistic simulations are under uniaxial tension or pure shear deformation, which is far from the actual situation where the micro or nano-components can be usually under mixed loading and multiple stress state. Very few authors have attempted to investigate the behavior and deformation mechanisms of nanocrystalline materials under multiple stress state at atomistic scale. Kitamura et al. [21] conducted numerical simulations to study the effect of transverse deformation on the fracture process of singlecrystal nickel, the simulation results shown that the constraint placed on the boundaries transverse to the uniaxial loading direction can lead to very high tensile yield stresses and severely limit inelastic deformation. Warner and Molinari [22] used the molecular dynamics (MD) simulation to probe the influence of normal loading on grain boundary shear response. They reported that the shear strengths of some grain

boundaries are correlated with normal stress acting on the interface. Spearot et al. [23, 24] have recently examined a range of geometries of single crystal Cu and symmetric tilt grain boundaries loaded on tension, and thus, the stress state on the active slip system was indirectly varied as crystallographic orientation changed. They were able to shown that the non-glide direction stress components acting on the slip plane can influence the partial dislocation nucleation process and the maximum tensile strength.

In this study, we conduct MD simulations to study the properties of deformation and fracture of nanocrystalline copper from the atomic point of view, both single crystal, bicrystal and polycrystal models are employed. Simulations are conducted firstly on a bicrystal and a polycrystal model without initial defects to investigate their mechanical properties and deformation behaviors. Then, a single crystal and a polycrystal model with a initial crack are numerically simulated to study the propagation of crack. In order to create different stress state, tensile strain are applied on each model with two different boundary conditions. The detailed information of simulation models and the boundary conditions will be specified in section 2. The simulation results are presented and discussed in section 3.

2. Simulation Method

2.1 Simulation model

Simulation models used in this study are presented in Fig.1. The bicrystal model with ∑5(3 1 0) grain boundary is created by constructing two separate crystals with different crystallographic orientation and joining them together along Y axial, as shown in Fig.1(a). The polycrystal model is generated using the Voronoi construction method with random grain sizes and random crystallographic orientations, as shown in Fig.1(b). It contains 27 grains with a mean grain size 9.1 nm. The single crystal model is arranged routinely with its three crystallographic orientation along the X, Y, Z coordinate axis respectively. An initially wedgy crack is inserted into the side of single crystal model, as shown in Fig.1(c). The same polycrystal model of Fig.1(b) with initial crack is shown in Fig.1(d). Periodic boundary conditions are applied along all directions (X, Y and Z) of the simulation models. It should be noted that periodic boundary condition in Y direction introduces a second boundary plane into the bicrystal model in Fig.1(b). The initial crack in Fig.1(c) and Fig.1 (d) can propagate on both sides of the models due to the periodic boundary condition in X direction.

Simulation models are prepared using a combination of molecular statics and MD simulations to obtain the equilibrium structures. Molecular statics calculations, which employ a nonlinear conjugate gradient method, are used to determine the minimum energy configurations. After the minimum energy configuration is attained, the simulation model is equilibrated using MD in the isobaric-isothermal (NPT) ensemble at a pressure of 0 bar and a temperature of 10 K for 20 ps. The dimension of the equilibrium models are present in Table.1. All the simulations in this study are performed with the LAMMPS code [25].

The interatomic potential chosen for simulations plays a profound role in the accurate prediction of defective structures. In this study, Copper is modeled using the embedded-atom method (EAM) potential developed by Mishin et al. [26]. The intrinsic stacking fault energies and unstable stacking fault energies from their simulation result are 44.4mJ/m^2 and 158mJ/m^2, respectively, which are very close to the experimental measurement 45mJ/m^2 [27] and 162mJ/m^2 [26].

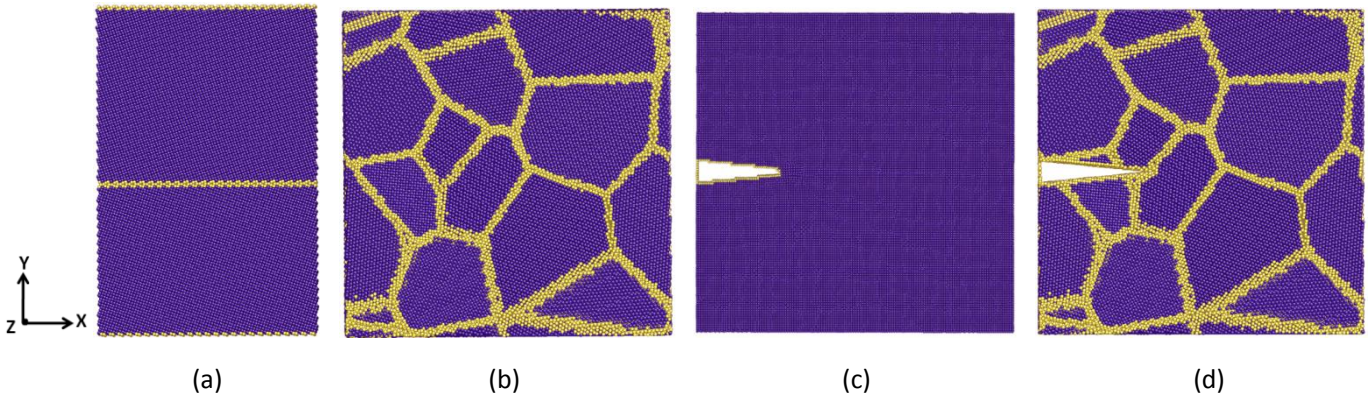

Fig.1 Equilibrium configuration of simulation models. (a) bicrystal (b) polycrystal (c) single crystal with initial crack (d) polycrystal with initial crack.

Table.1 Dimension of simulation models

Simulation model	Model dimensions X×Y×Z (Å)	Number of atoms
Bicrystal	144.4×218.4×108.3	285,000
Polycrystal	216.6×216.6×216.6	832,750
Single crystal with crack	216.6×216.6×216.6	850,744
Polycrystal with crack	216.6×216.6×216.6	821,367

2.2 Boundary conditions of tensile loading

The simulation models are subjected to a tensile deformation along Y direction at a constant strain rate of $1\times10^{9}s^{-1}$. An integration time step of 1.0 fs is adopted throughout the MD simulations. The temperature is set at 10 K at the initial in every tension step to avoid the influence of the thermal motion of atoms at high temperature. In order to create different stress state, two different boundary conditions are used in this work. Specifically, MD simulations are performed using either 'free' or 'constrained' tension boundary conditions, as schemed in Fig.2. For the free tension boundary condition, the boundaries in the lateral directions are allowed to expand or contract during the deformation process so that the transverse stress are kept free ($\sigma_{xx} = \sigma_{zz} = 0$), as shown in Fig.2(a). For the constrained tension boundary condition, computational models are strained at a constant rate along the Y axis while keeping fixed the model dimensions along the X and Z directions. The lateral boundaries are constrained by not allowing the periodic simulation model to expand or contract during the deformation process ($\varepsilon_{xx} = \varepsilon_{zz} = 0$), as shown in Fig.2(b). This boundary condition consider the transverse stress along the X and Z directions during the tensile deformation. The dashed lines in Fig.2 represent the initial shape of the model, while the solid lines represent the deformed shape. These boundary conditions are very similar to those used by Kitamura et al. [21] and Spearot et al. [28] to study the effect of boundary condition on tensile deformation of nickel single crystal and copper bicrystal respectively.

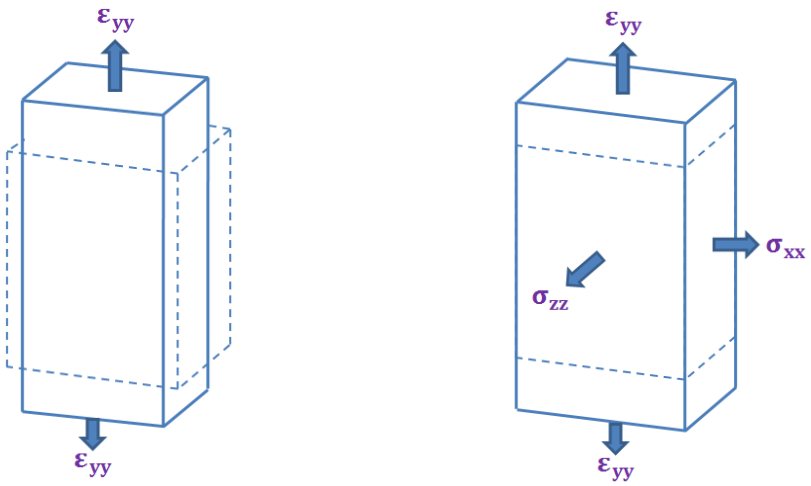

Fig.2 Schematic of simulation model with two different tension boundary conditions. (a) free tension boundary condition (b) constrained tension boundary condition. (Reference Fig.2 in [21])

In order to further validate the Mishin et al. EAM potentials [26] and the molecular dynamics code, simulations are designed to calculate the elastic stiffness (C_{11} and C_{12}) of Cu single crystal model. As introduced above, the displacement (or strain) in X and Z directions is equal to zero under constrained tension boundary condition. Thus, the set of elastic equations to describe the response of a homogeneous cubic crystal,

$$\begin{bmatrix}\sigma_1\\ \sigma_2\\ \sigma_3\\ \sigma_4\\ \sigma_5\\ \sigma_6\end{bmatrix} = \begin{bmatrix}C_{11} & C_{12} & C_{12} & & & \\ C_{12} & C_{11} & C_{12} & & & \\ C_{12} & C_{12} & C_{11} & & & \\ & & & C_{44} & & \\ & & & & C_{44} & \\ & & & & & C_{44}\end{bmatrix}\begin{bmatrix}\varepsilon_1\\ \varepsilon_2\\ \varepsilon_3\\ \varepsilon_4\\ \varepsilon_5\\ \varepsilon_6\end{bmatrix} \quad (1)$$

reduces to ,

$$\sigma_1=C_{12}\varepsilon_2=\sigma_3 \quad (2)$$

$$\sigma_2=C_{11}\varepsilon_2 \quad (3)$$

Thus, the elastic constants C_{11} and C_{12} can be determined by measuring the slope of the appropriate stress-strain relation. For the mechanical properties, the system stress is attained by calculating the pressure of the entire system of atoms. The pressure is computed by the formula

$$P_{ij} = \frac{1}{V}\left[\sum_k^N m_k v_{k_i} v_{k_j} + \sum_k^N r_{k_i} f_{k_j}\right], (i, j=x, y, z) \quad (4)$$

where the first term uses components of the kinetic energy tensor and the second term uses components of the virial tensor. *N* is the total number of atoms in the simulation model, *V* is the simulation model volume. *r* and *f* is the force vector and the distance vector respectively. System strain is derived from the positions of the periodic boundaries. The elastic constants calculated from the initial slope of the MD simulations are 173.2GPa and 124.8GPa, which are all within acceptable accuracy of the experimental values of 168.4GPa and 121.4 GPa [29].

In addition, only principle stress is applied in our study, as shown in Fig.2, the well established von Mises yield criterion can be described as following,

$$\sigma_v = \sqrt{\frac{1}{2}\left[(\sigma_1-\sigma_2)^2 + (\sigma_1-\sigma_3)^2 + (\sigma_2-\sigma_3)^2\right]} \quad (5)$$

In the case of free tension boundary condition ($\sigma_1 = \sigma_3 = 0$), the von Mises criterion simply reduces to,

$$\sigma_v=\sigma_2 \quad (6)$$

which means the material starts to yield when σ_2 reaches the yield strength of the material σ_v, and is in agreement with the definition of tensile yield strength. On the other hand, in the case of constrained tension boundary condition ($\sigma_2 > \sigma_1 = \sigma_3 \neq 0$), the von Mises criterion can expressed as,

$$\sigma_v=\sigma_2-\sigma_1=\sigma_2-\sigma_3 \quad (7)$$

From equation (6) and (7), we can deduce that the simulation model starts to yield at a higher tensile stress (σ_2) under constrained boundary condition than the value under free boundary condition. Actually, this deduction is confirmed in our MD simulation, which will be specified in section 3.

3. Simulation Results

3.1 Tensile response of Cu bicrystal and polycrystal

Fig.3 shows the tensile stress-strain response for Cu bicrystal model with ∑5(3 1 0) grain boundary subject to a tensile deformation under two different tension boundary conditions. The maximum tensile stress corresponds to the nucleation of partial dislocations, in agreement with results for uniaxial tensile of Cu bicrystal by Spearot et al. [30, 31]. The tensile stress required for dislocation emission of bicrystal model under constrained boundary condition is 13.47 GPa, which is significantly higher than that required under free boundary condition (4.72 GPa). Apparently, the difference of the maximum tensile strength is result from the stresses that developed transverse to the loading direction during the deformation process. The result is conform to our deduction from the Mises yield criterion.

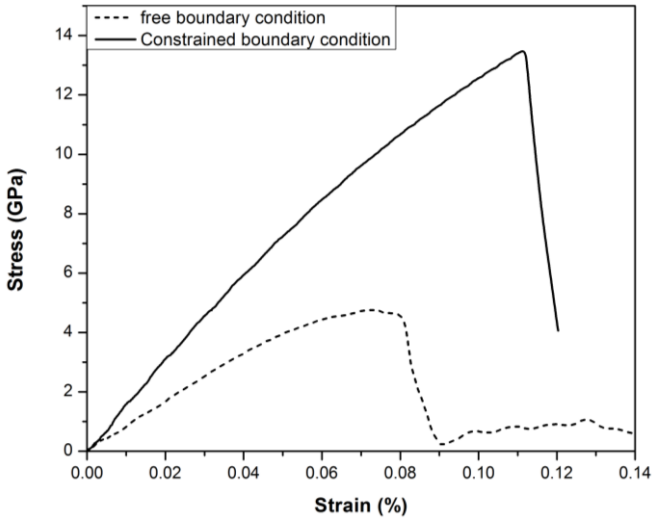

Fig.3 Relationship between stress and strain of Cu bicrystal model under two different tension boundary conditions.

To gain fundamental understanding of the strength differences between two different tension boundary conditions, the deformation mechanisms at atomistic scale are examined, as shown in Fig.4 and Fig.5. The atomic mechanisms are determined by examining continuous snapshots stored during the MD simulation. All images are colored according to the common neighbor analysis (CNA) parameter [32]. Atoms with perfect fcc structures are removed to facilitate viewing of the defect structures. Atoms colored with bright green organize the grain boundary plane and the dislocation core, while the blue atoms correspond to the hcp structures represent stacking fault.

Fig.4(a) and Fig.5(a) show the snapshot of atoms in the bicrystal model at the beginning of the stress drop under free boundary condition (ε=0.08) and constrained boundary condition (ε=0.112) respectively. Images indicate that partial dislocations with both edge and screw character are nucleated from the bicrystal interface once the maximum tensile stress has been reached, regardless of whether free or constrained tension boundary condition are prescribed. In addition, the constrained boundary condition promote the nucleation of crack along the grain boundary plane due to the local cleavage fracture at the stress drop, as shown in Fig.5(b) at ε=0.118. The crack propagates rapidly along the boundary plane and eventually result in the cleavage of the two grains of the bicrystal model. During the deformation process under constrained boundary condition, a limited number of dislocations nucleated from the boundary plane which restrict the plastic deformation and caused the brittle behavior of the bicrystal model, as seen of the sudden drop of the stress curve in Fig.3. This is different from the case under free boundary condition, where dislocation nucleation and propagation dominant the deformation mechanisms during the whole process of the simulation without any crack nucleation, as shown in Fig.4(b) at ε=0.082 or even at a higher strain rate, although it is not shown here.

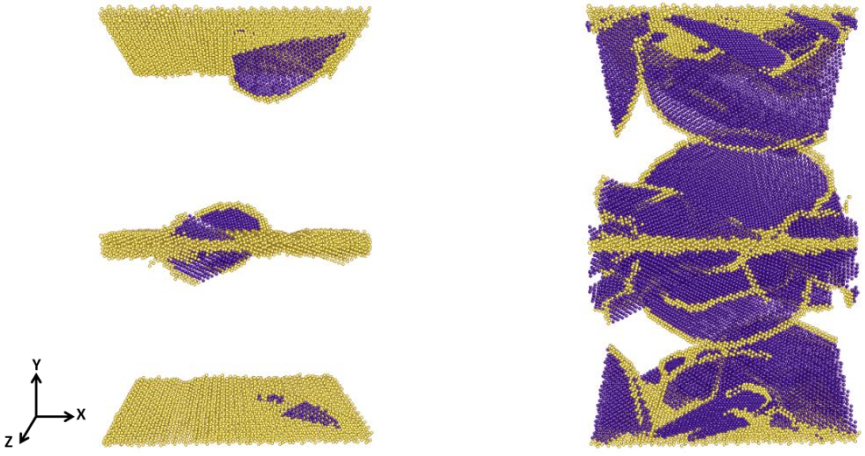

(a) ε=0.08 (b) ε=0.082

Fig.4 (Color online) Snapshots of copper bicrystal model at different tensile strain rate under free tension boundary condition at 10 K.

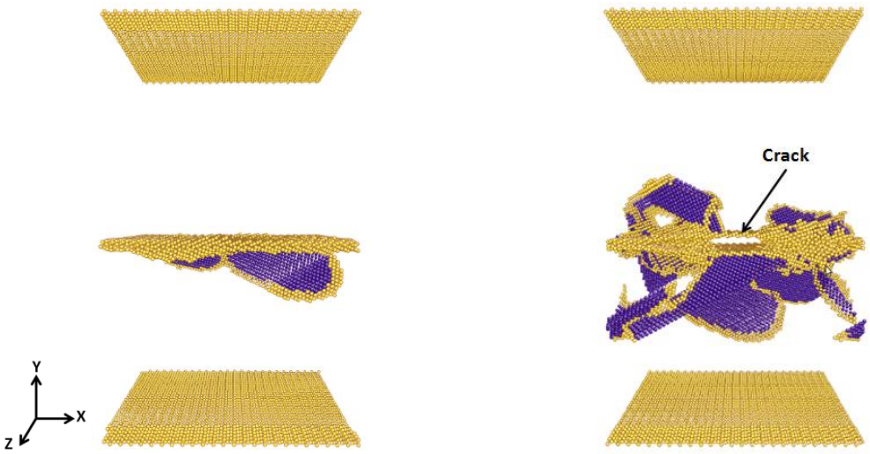

(a) ε=0.112 (b) ε=0.118

Fig.5 (Color online) Snapshots of copper bicrystal model at different tensile strain rate under constrained tension boundary condition at 10 K.

The relationship between stress and strain of polycrystal Cu under two different tension boundary conditions are plotted in Fig.6. Under constrained boundary condition, the maximum tensile stress reaches 9.26 GPa, being much higher than the value under free boundary condition (2.13 GPa) without the transverse stress, which is conform to our deduction based on the Mises yield criterion. Fig.7 shows the atomic configuration of Cu polycrystal model at different tensile strain rate. Dark blue, bright green and light blue atoms correspond to the local fcc, defect and hcp structures classified by CNA, respectively. Under constrained boundary condition, some grain boundaries become coarsening when deformation is performed. Meanwhile, voids are nucleated along the grain boundaries after several dislocations have been emitted from the boundary plane, as shown in the snapshot of Fig.7(b) at ε=0.055. The nucleated voids grow and coalesce during the deformation process and eventually leading to complete fracture of the model. Recall that, the mechanical response and deformation mechanisms of Cu polycrystal under constrained condition are quite similar to that described in Cu bicrystal model previously under the same condition.

The brittle behavior without obvious plastic strain under constrained boundary condition is completely different from the ductile one under free boundary condition where the slip deformation mechanism dominant the process. Massive dislocations nucleate from the grain boundary plane on one side and propagate across the grains and eventually be absorbed by the grain boundaries on the other side, leaving many stacking faults in the grains. Dislocation interaction is also prevail in the Cu polycrystal, as shown in Fig.6(a). The result is comparable with the previous simulation work on Cu polycrystal model under uniaxial tension [33-35] and in agreement with other fcc metals with low stacking fault energy in the experiments [36, 37]. Note that, no voids are nucleated during the tensile deformation under free condition even at a high strain rate of ε=0.1, see in Fig.6(a). The dislocation mediate deformation mechanism under free boundary condition contribute the ductile behavior of polycrystal Cu model and result in the stress flow in Fig.6.

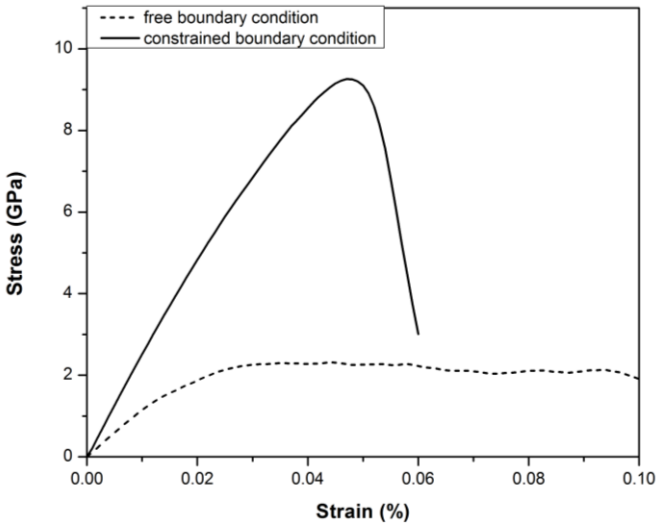

Fig.6 Relationship between stress and strain of Cu polycrystal model under two different tension boundary conditions.

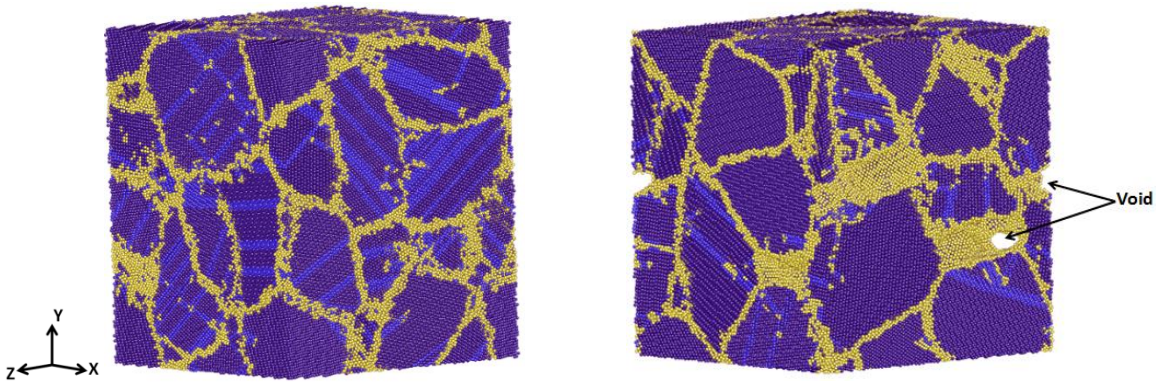

(a) ε=0.1 (b) ε=0.055

Fig.7 (Color online) Snapshots of copper polycrystal model at different tensile strain using (a) free tension boundary condition (b) constrained tension boundary condition at 10 K.

3.2 Crack evolution in Cu single crystal and polycrystal

Fig.8 and Fig.9 give the details of the atomistic process of the crack evolution in Cu single crystal under two different tension boundary conditions. In the case of free boundary condition, the initial crack-tip blunting occurred with the increase of tensile deformation. However, the crack propagation is not obvious even when the tensile strain reaches ε=0.07, as seen in Fig.8(a). There is a plastic region in front of the crack-tip, and the atoms in this region are disordered rather than keeping the initial fcc structure. The stress increases and then concentrates itself at the crack-tip and result in the nucleation of dislocation at this region, as indicated in Fig.8(a). Note that, periodic boundary condition is applied on the X axis, as the applied strain increasing, the crack blunting increase on both side of the initial crack and consecutive dislocations are emitted from the crack frontier, as seen in Fig.8(b) and Fig.8(c).

Under constrained boundary condition, the crack propagate forward rapidly along the [1 0 0] direction, driven by something like a brittle manner. Atoms are still well ordered and no dislocation is emitted in the front of crack-tip, as seen in Fig.9(a) at ε=0.05. Crack propagation mechanisms involved only fatigue cleavage of atomic bonds in the crack plane leading to crack extension. At ε=0.06 in Fig.9(b), the plastic region appeared at the crack frontier and dislocations nucleated on both side of the crack, which is similar to the mechanism in Fig.8(b). But different from the case under free boundary condition, where dislocation nucleation and slipping accommodate the plastic deformation, with the increased tensile strain, the crack keeps propagating forward in a cleavage manner and eventually result in the fracture of the model. Only a limited number of dislocations are nucleated during the tensile deformation.

It is worth noting that, the fracture of Cu single crystal in a brittle manner under constrained boundary condition is just

one case since the single crystal model in this study is routinely arranged and the initial crack-tip is inserted on the (0 0 1) plane. Actually, many deformation parameters should be taken into consideration when examining the brittle or ductile fracture mechanism in the simulation work: temperature, strain rate, shape of the created crack, oriented misorientation of grain atoms, the mode of force applied and its value, etc. For example, Potirniche and coworkers [38] investigate the influence of crystallographic orientation on the crack growth path in single crystal Cu. In their MD simulation, the crack-tip plasticity is determined by the number of active slip system resulting from the different orientations, both crack-tip blunting and fatigue cleavage was observed. In any case, the stress state is determined in our simulation to be a another significant factor that can affect the crack evolution in the bulk materials.

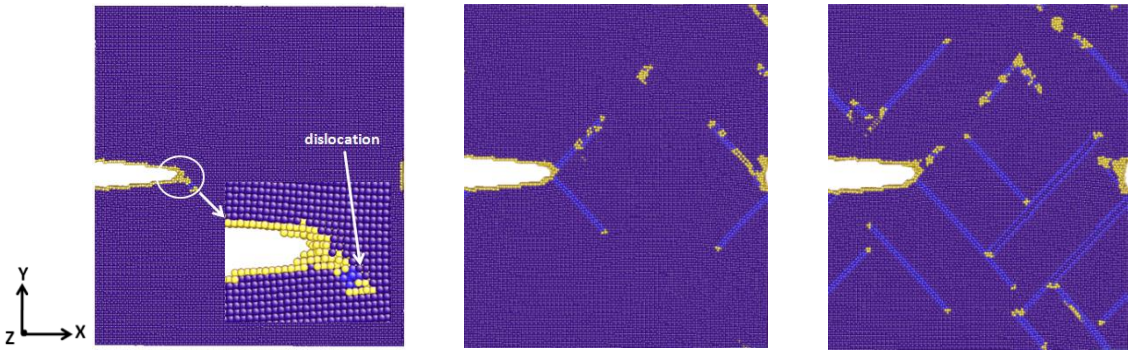

(a) ε=0.07 (b) ε=0.086 (c) ε=0.09

Fig.8 (Color online) Atomic configurations of cross sections of copper single crystal model with initial crack at different tensile strain rate under free tension boundary condition at 10 K.

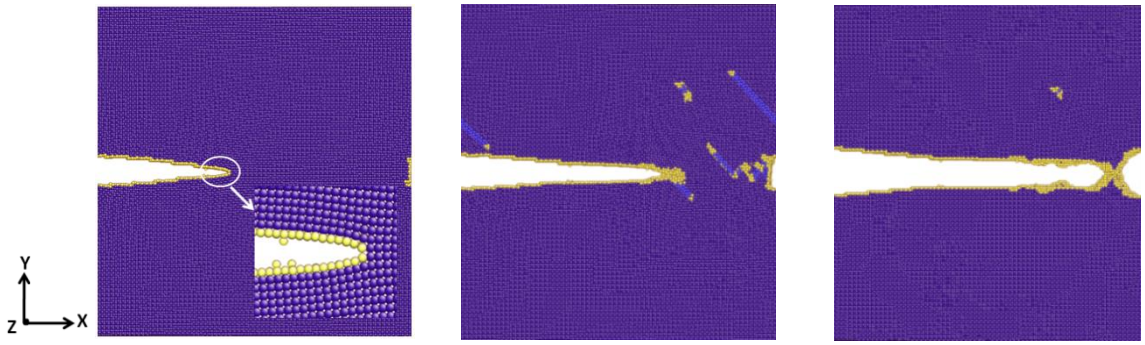

(a) ε=0.05 (b) ε=0.06 (c) ε=0.09

Fig.9 (Color online) Atomic configurations of cross sections of copper single crystal model with initial crack at different tensile strain rate under constrained tension boundary condition at 10 K.

Fig.10 and Fig.11 present the atomistic process of the crack evolution of polycrystal Cu under two tension boundary conditions. At ε=0.01, crack keeps its original configuration under free boundary condition, some embryo partial dislocation nucleated from grain boundary near the crack-tip region in grain 1, as seen in Fig.10(a). With the increase of applied tensile deformation, massive dislocations are emitted from the grain boundaries in each grain and travel through the grains to the opposite grain boundaries, as shown in Fig.10(b). The initial inserted crack seems play a little role during the deformation process since the crack-tip didn't propagate forward and no conspicuous crack blunting is observed in this case. Similar to the case of single crystal, dislocation mediated plastic deformation is the dominant mechanism of the Cu polycrystal under free boundary condition.

Under constrained boundary condition, as shown in Fig.11(a), the crack becomes blunt compared with its initial configuration and has been propagating forward a small distance when the applied tensile strain reaches ε=0.01. No embryo dislocation near the grain boundaries was observed at this stage. What's interesting is that, with the increasing of the tensile strain, the crack-tip didn't propagate forward in a brittle fracture manner as expected as its evolution in the single crystal model. Instead, the crack-tip became significant blunt and the crack extended along the grain boundaries nearby. The

intergranular fracture in this case is different from the intragranular fracture in our previous result [39], which can be ascribed to the location of the initial crack. The crack-tip in our previous simulation is arranged inside the grain and far from the nearest grain boundary, while in this work, the crack-tip is inserted at the grain boundary place, as shown in Fig.1(a). From the comparison of the crack performance between polycrystal model with single crystal model under constrained boundary condition and with our former simulation result, two conclusions can be implied here. For one thing, the crystallographic orientation of grain on the crack growth path have a strong impact on the crack propogation. For the other, grain boundary is the preferential path of the crack extension since the atoms on the boundary plane have higher energy and are more easier to diffuse.

In addition, massive dislocation are observed in polycrystal Cu under constrained boundary condition at ε=0.08. Note that, under the free boundary condition, dislocations are first nucleated from one side of each grain and then propagate along the same slip plane to the opposite side, seen in Fig.10(b). However, under constrained boundary condition, the transverse stress activates more slip systems so that dislocations can be nucleated from different grain boundaries in each grain and slip on different slip planes, as shown in Fig.11(b). The propagation of dislocations on different slip system can induce relative sliding between two neighboring grains [35], and grain rotation occurs as a result of cooperative sliding along the opposite boundaries of the grain. For example, grain 1 and grain 2 in Fig.11(a) have different crystallographic orientation at ε=0.01, but the relative rotation of the two grains changes their initial orientation gradually and eventually result in the combination of the two grains at ε=0.08, as shown in Fig.11(b). Moreover, the rotation of grains can also lead to the separation of the grain, as seen in Fig.11, grain 3 split into two grains at ε=0.08. The grain rotation induced grain separation or combination are not observed in other grains of the polycrystal at ε=0.08, this is mainly because that small grains rotate much faster than larger ones [35]. Furthermore, grain boundary migration which are reported previously [40, 41] is not obviously seen at ε=0.08 under both of the two tension boundary conditions, this is mainly because of the low temperature used in our simulation and the accumulated local stress may not high enough to drive the motion of the grain boundaries [42, 43].

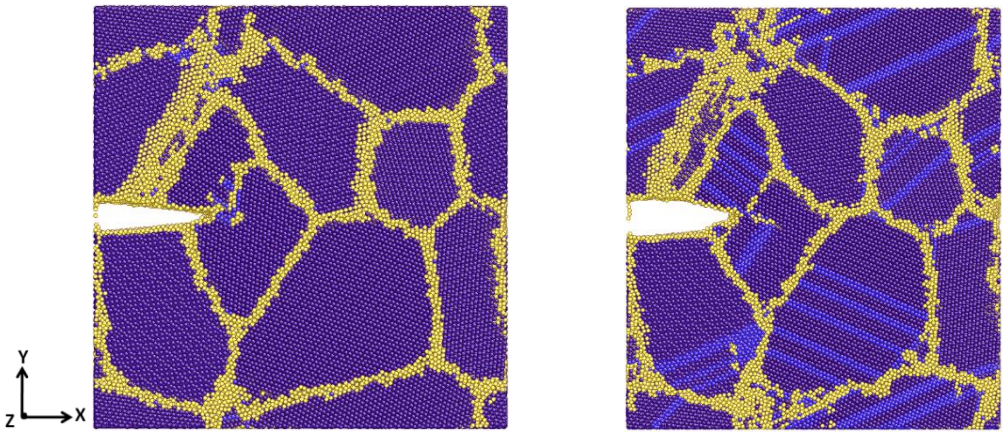

(a) ε=0.01 (b) ε=0.08

Fig.10 (Color online) Atomic configurations of cross sections of copper polycrystal model with initial crack at different tensile strain rate under free tension boundary condition at 10 K.

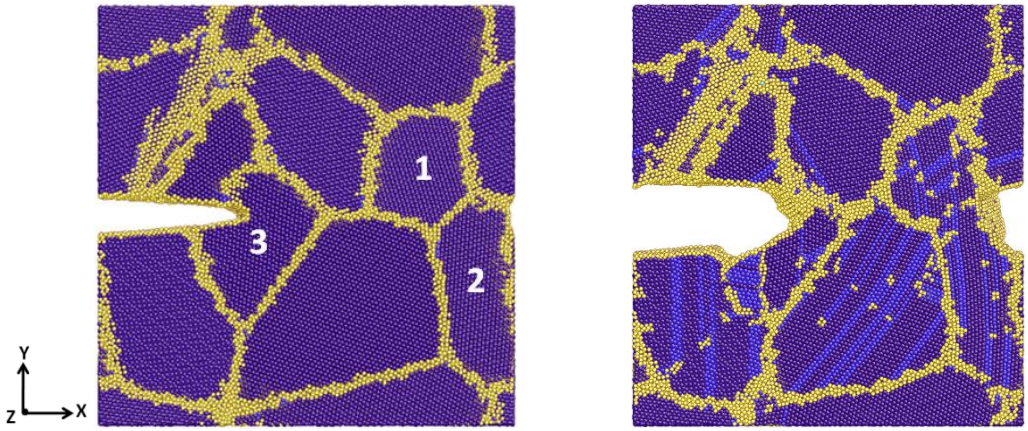

(a) ε=0.01 (b) ε=0.08

Fig.11 (Color online) Atomic configurations of cross sections of copper polycrystal model with initial crack at different tensile strain rate under free tension boundary condition at 10 K.

4. Conclusions

The mechanism of deformation and fracture of Cu single crystal, bicrystal and polycrystal has been studied at the nanoscale under two different tension boundary conditions using MD simulations. As a whole, this work demonstrates that stress state is particularly important in determining mechanical properties and fatigue resistance in materials. The results are summarized as follows.

(1) For the Cu bicrystal and polycrystal models, the tensile stress required for dislocation emission for the bicrystal and polycrystal under constrained boundary condition are significant higher than that required under free boundary condition. The failure of models is dominated solely by partial dislocation slip activity under the free boundary condition, while under constrained boundary condition, the multistate of tensile stress due to the transverse stress perpendicular to the tensile axial leads to a more brittle mode of failure.

(2) The evolution of crack in the Cu single crystal model under two tension boundary conditions are completely different. Under free boundary condition, the emission of dislocations from the crack-tip and their propagation is the dominant mechanism during the tensile deformation. The deformation mechanism is quite another thing under the constrained boundary condition, where the crack extends along the [1 0 0] direction in a cleavage manner and eventually result in the fracture of the model.

(3) Under free boundary condition, crack plays a little role during the tensile deformation of Cu polycrystal in this study, dislocation nucleation from grain boundary and its propagation in the grain is the dominant mechanism. Under constrained boundary condition, grain boundaries hinder the propagation of the crack-tip but provide the path for the extension of the crack. In addition, the principle tensile stress along with the transverse stress can activate multiple slip systems in each grain of Cu polycrystal.

Acknowledgements

Simulations were performed using the HPC cluster of University of Wollongong and the computing facilities provided by NCI National Facility of Australia. L. Zhang, L.Q. Pei and X. Zhao would like to acknowledge the financial support from China Scholarship Council (CSC).

References

[1] M Dao, L Lu, R J Asaro, J T M De Hosson, E Ma 2007 *Acta Mater.* **55** 4041.

[2] Weertman 1999 *MRS Bull.* **24** 44.

[3] Z N Farhat, Y Ding, D O Northwood, A T Alpas 1996 *Mater. Sci. Eng. A* **206** 302.

[4] D H Jeong, F Gonzalez, G Palumbo, K T Aust, U Erb 2001 *Scr. Mater.* **44** 493.

[5] T J Rupert, C A Schuh 2010 *Acta Mater.* **58** 4137.

[6] T Hanlon, E D Tabachnikova, S Suresh 2005 *Int. J. Fatigue* **27** 1147.

[7] P Cavaliere 2009 *Int. J. Fatigue* **31** 1476.

[8] J J Xie, Y S Hong 2009 *Acta Metall. Sin.* **45** 844.

[9] W Ya-Bin, Z Gang, L Ming-Jie, C Xiang-Long, C Jun 2009 *Chin. Phys. B* **18** 1181.

[10] S F Xie, S D Chen, A K Soh 2011 *Chin. Phys. Lett.* **28** 066201.

[11] D Wolf, V Yamakov, S R Phillpot, A Mukherjee, H Gleiter 2005 *Acta Mater.* **53** 1.

[12] J Schiotz, F D Di Tolla, K W Jacobsen 1998 *Nature* **391** 561.

[13] H Van Swygenhoven, M Spaczer, A Caro, D Farkas 1999 *Phys. Rev. B* **60** 22.

[14] H Van Swygenhoven, P M Derlet 2001 *Phys. Rev. B* **64** 224105.

[15] V Yamakov, D Wolf, M Salazar, S R Phillpot, H Gleiter 2001 *Acta Mater.* **49** 2713.

[16] H Van Swygenhoven, P M Derlet, A G Frøseth 2006 *Acta Mater.* **54** 1975.

[17] F Sansoz, J F Molinari 2005 *Acta Mater.* **53** 1931.

[18] Z Yu-Ming, H Yi-Gang, L Ai-Xia, W Qing 2009 *Chin. Phys. B* **18** 3966.

[19] W Tun, Z Fu-Xin, L Yue-Wu, 2001 *Chin. Phys. Lett.* **18** 1242.

[20] A P Sutton, R W Balluffi 1995 *Interfaces in crystalline materials* (Oxford: Cambridge University Press) 205.

[21] T Kitamura, K Yashiro, R Ohtani 1997 *JSME Int. J. Series A* **40** 430.

[22] D H Warner, J F Molinari 2008 *Model. Simul. Mater. Sci. Eng.* **16** 705.

[23] D E Spearot, M A Tschopp, K I Jacob, D L McDowell 2007 *Acta Mater.* **55** 075007.

[24] M A Tschopp, D L McDowell 2007 *Appl. Phys. Lett.* **75** 121916.

[25] S Plimpton 1995 *J. Comput. Phys.* **117** 1.

[26] Y Mishin, M J Mehl, D A Papaconstantopoulos, A F Voter, J D Kress 2001 *Phys. Rev. B* **63** 2241061.

[27] C B Carter, I L F Ray 1977 *Philos. Mag.* **35** 189.

[28] D E Spearot 2008 *Mech. Res. Commun.* **35** 81.

[29] R W Hertzberg *Deformation and fracture mechanics of engineering materials* (New York: J. Wiley & Sons).

[30] D E Spearot, K I Jacob, D L McDowell 2007 *Int. J. Plasticity* **23** 143.

[31] M A Tschopp, D L McDowell 2008 *Int. J. Plasticity* **24** 191.

[32] J Schiøtz, F D Di Tolla, K W Jacobsen 1998 *Nature* **391** 561.

[33] H Van Swygenhoven, J R Weertman 2006 *Mater. Today* **9** 24.

[34] T Shimokawa, A Nakatani, H Kitagawa 2004 *JSME Int. J. Series A*, **47** 83.

[35] Y G Zheng, H W Zhang, Z Chen, C Lu, Y W Mai 2009 *Phys. Lett. A* **373** 570.

[36] T Kizuka 1998 *Phys. Rev. B* **57** 11158.

[37] K Furuya, K Mitsuishi, N Ishikawa, C W Allen 2000 *Mater. Sci. Eng. A* **285** 85.

[38] G P Potirniche, M F Horstemeyer, P M Gullett, B Jelinek 2006 *Proc. R. Soc. A* **462** 3707.

[39] P Lin Qing, L Cheng, T Kiet, Z Hong Tao, Z Xing, C Kui Yu, Z Liang 2013 *J. Nano Res.* **25** 188.

[40] M Legros, D S Gianola, K J Hemker 2008 *Acta Mater.* **56** 3380.

[41] K L Merkle, L J Thompson, F Phillipp 2004 *Interface Sci.***12** 277.

[42] A J Haslam, D Moldovan, V Yamakov, D Wolf, S R Phillpot, H Gleiter 2003 *Acta Mater.* **51** 2097.

[43] M Shiga, W Shinoda 2004 *Phys. Rev. B*, **70** 054102.